International Journal of Remote Sensing
Vol. 32, No. 5, 10 March 2011, 1303–1318

Taylor & Francis
Taylor & Francis Group

Quantification of non-homogeneity from ocean remote-sensing images using two-dimensional continuous wavelet transforms

LI-CHUNG WU†, LAURENCE ZSU-HSIN CHUANG*‡, DONG-JIING DOONG§ and CHIA CHUEN KAO†

†Department of Hydraulic and Ocean Engineering, National Cheng Kung University, Taiwan, ROC

‡Institute of Ocean Technology and Marine Affairs, National Cheng Kung University, Taiwan, ROC

§Department of Marine Environmental Informatics, National Taiwan Ocean University, Taiwan, ROC

(*Received 9 June 2008; in final form 17 November 2009*)

In this study, a two-dimensional continuous wavelet transform is applied to quantify the non-homogeneity from remote-sensing wave images. Our study shows that the non-homogeneity index, which is proposed here, is capable of identifying the degree of non-homogeneity from the wave-field images. However, the influence from the edges of the wave-field image should be considered in analysis. The calculated results from the simulated wave fields and from the natural wave-field images reveal that the non-homogeneity index is influenced by the bathymetry inside the area of the ocean-wave image. It conforms to the character of the natural wave non-homogeneity. After discussing the wave characteristics from the wave-field image with a high non-homogeneity index, an inhomogeneous algorithm is recommended for obtaining accurate and reasonable wave results from the wave image.

1. Introduction

Ocean-wave information is the basis for performance improvements of ocean and coastal activities. Navigation, harbour construction, fishing and cultivation, coastal disaster protection, recreation and even defence capabilities have become much more dependent on the availability of long-term, stable and high-quality oceanographic information. Ocean-wave observation always plays an important role in evaluating and describing wave characteristics. Wave energy, wave period, wavenumber and wave direction are the keys for understanding of the mechanisms of wave formation and propagation. These (wave energy, wave period, wavenumber and wave direction) are also what we observed for the purposes of ocean and coastal activities. At present, various in-situ measurements with single-point sensors have been developed significantly; they are designed to collect wave information from the time domain. Remote sensing is a useful method to observe wave features in the space domain. Some studies have revealed the possibility of observing waves by remote-sensing technologies (Vachon and West 1992, Turiel *et al.* 2007).

A wave image spectrum is the key to calculating the wave parameters from an ocean remote-sensing image (Alpers and Hasselmann 1978). Wave features, such as

*Corresponding author. Email: laurence.chuang@gmail.com

International Journal of Remote Sensing
ISSN 0143-1161 print/ISSN 1366-5901 online
http://www.tandf.co.uk/journals
DOI: 10.1080/01431160903547957

wavenumber and wave direction, are obtained from the wave image spectrum (Kuo *et al.* 1999). In order to derive the wave image spectrum from the ocean remote-sensing image, a given range of sub-image was analysed by means of spectrum algorithms. Nowadays, Fourier transforms have been popularly adopted in ocean remote-sensing image analysis for obtaining the wave image spectrum (Kanevsky 2005). To apply Fourier transforms in the image analysis, the assumption of spatial homogeneity within the analysed area is necessary. However, it is a fact that most real signals in the nature are inhomogeneous or nearly inhomogeneous, as are the wave signals from remote-sensing images, especially for the wave-field images from coastal areas or near the shore. Due to the influences of the variant bathymetry and coastal structures, ocean waves would always be transformed in space (Reeve *et al.* 2004). It is almost impossible to assume that the wave-field images near the shore are homogeneous because of the change of wave features in the space domain.

In order to analyse the inhomogeneous wave-field images, a short-time Fourier transform (STFT) can be applied. The solution to inserting space information into the spatial frequency domain of the signal is to divide the signal into small windows so that the signal can be assumed to be homogeneous inside the range of the window. For each such window, the Fourier transform can be applied. In contrast to the Fourier transform, the window is of finite size in the window Fourier transform, resulting in imperfect frequency resolution. If it is assumed that the size of the window is infinite, as it is in the Fourier transform, a perfect spatial frequency resolution is obtained whilst the space information is lost. The selection of the proper window width is related to what is known as the Heisenberg Uncertainty Principle (Van Name 1960). It is not known what spectral components exist in what instances of space. Narrow windows provide good space resolution, but poor spatial frequency resolution. Wide windows provide good spatial frequency resolution, but poor space resolution. Furthermore, wide windows may violate the very condition of the signal as stationary or homogeneous. Hence, to obtain complete and reliable wave information from the inhomogeneous wave image, it is necessary to determine the homogeneous window from the whole inhomogeneous image.

The method to quantify the inhomogeneity from the wave image is essential to determine the areas or windows from the entire inhomogeneous image. Some studies have focused on the issue of quantifying the homogeneity from the signals in nature. Mountain and Birnbaum (1982) proposed a method to determine the non-homogeneity size and shape from the scattering of low-frequency sound waves in a solid. Some parameters, which cannot be calculated from the remote-sensing images, are necessary to input into the algorithm. It is difficult to apply it to remote-sensing image analysis. Liu (2000) applied the one-dimensional continuous wavelet transform (CWT) to determine the degree of non-stationarity from different kinds of time series of signals. The CWT is now recognized as a useful, flexible and efficient technique to analyse intermittent, non-stationary and inhomogeneous signals, as well as images that are obtained from experimental or in-situ measurements. It has been applied to solve a variety of engineering problems and almost every corner of physics. However, the implementations of the wavelet transform in one dimension (signal analysis) and in two dimensions (image processing) are quite different. It is the purpose of this article to develop a procedure for quantifying the non-homogeneity from the ocean remote-sensing images by implementing the two-dimensional (2-D) CWT, so as to determine the degree of the non-homogeneity. The simulated and natural wave images are both used to verify the practicability of the algorithm.

2. Theoretical preliminaries

'Homogeneity' implies that the statistical properties do not change with space. For the mathematical definition of homogeneity or stationarity, $\{X_t\}$ is said to be completely stationary if the joint probability distribution of $\{X_{t1}, X_{t2}, ..., X_{tn}\}$ is identical to that of $\{X_{t1+k}, X_{t2+k}, ..., X_{tn+k}\}$ (Priestley 1991). In this paper, we have used the 2-D CWT to calculate the non-homogeneity degree from the ocean-wave remote-sensing images. The algorithm is discussed in the following.

2.1 *Two-dimensional continuous wavelet transform (2-D CWT)*

As far as the principle of 2-D CWT is concerned, it assumes that various wavelets, which are scaled, rotated and shifted versions of a pre-chosen mother wavelet function, can be accumulated as any 2-D image signal (figure 1).

Given a two-dimensional spatial image $s(\boldsymbol{x}) = s(x, y)$ of finite energy, we can represent the analysed image by

$$\|s\|^2 = \int_{R^2} |s(\boldsymbol{x})|^2 d^2\boldsymbol{x} < \infty. \tag{1}$$

in which R^2 means two-dimensional space domain. In practice, the discrete values of $s(\boldsymbol{x})$ correspond to the level of grey of each pixel. The 2-D CWT $W(\boldsymbol{b},\theta,a)$ of the image function $s(\boldsymbol{x})$ with respect to a transformed mother wavelet $\psi_{\boldsymbol{b},\theta,a}$ is shown in (Antoine *et al.* 2004)

$$W(\boldsymbol{b}, \theta, a) = \frac{1}{\sqrt{C_\psi}} \langle \psi_{\boldsymbol{b},\theta,a} | s(\boldsymbol{x}) \rangle, \tag{2}$$

in which the constant C_ψ is associated with the admissibility condition and depends on the wavelet family (Antoine *et al.* 2004), and the function $\psi_{\boldsymbol{b},\theta,a}$ is the wavelet function,

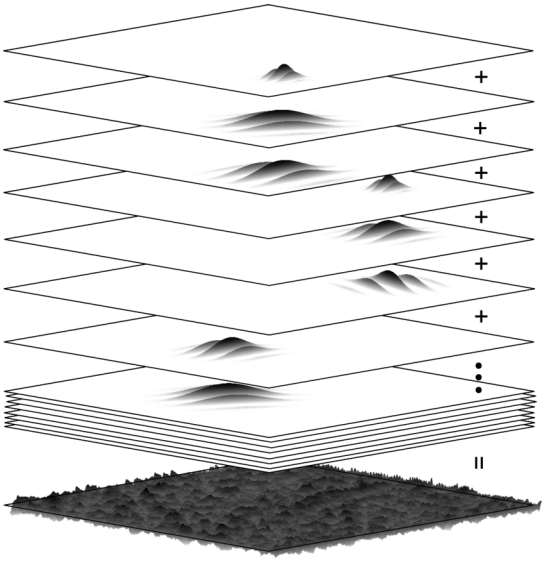

Figure 1. A schematic illustration of a wave image broken into various wavelets.

which is derived from the mother wavelet function ψ via dilations (a), translations ($\boldsymbol{b}$) and rotations ($\mathbf{r}_{-\theta}$):

$$\psi_{\boldsymbol{b},\theta,a} = a^{-1}\psi\left(a^{-1}\mathbf{r}_{-\theta}(\boldsymbol{x}-\boldsymbol{b})\right). \tag{3}$$

In equation (3), the factor a is a normalization that gives all dilated versions of the mother wavelet the same energy, i.e. it is the ratio of the size of the dilated wavelet to the size of the mother wavelet. The translation parameter $\boldsymbol{b}$ corresponds to the position of the wavelet as it shifts through the space domain. The rotation matrix $\mathbf{r}_{-\theta}$ with a rotation angle θ rotates the wavelet in spatial coordinates:

$$\mathbf{r}_{-\theta} = \begin{bmatrix} \cos\theta & \sin\theta \\ -\sin\theta & \cos\theta \end{bmatrix}, \quad 0 \le \theta < 2\pi\,. \tag{4}$$

The relationship between the mother wavelet function ψ and the wavelet function $\psi_{\boldsymbol{b},\theta,a}$ is shown in figure 2.

In equation (2), $W(\boldsymbol{b},\theta,a)$ conserves the norm of the signal, thus its total energy is

$$\int\int\int |W(\boldsymbol{b},\theta,a)|^2 \frac{da}{a^3} d^2\boldsymbol{b} = \int_{R^2} |s(\boldsymbol{x})|^2 d^2\boldsymbol{x}. \tag{5}$$

To better understand, equation (2) can be expressed as:

$$W(\boldsymbol{b},\theta,a) = C_\psi^{-1/2} a^{-1} \int_{R^2} \psi^*\left(a^{-1}\mathbf{r}_{-\theta}(\boldsymbol{x}-\boldsymbol{b})\right) s(\boldsymbol{x}) d^2\boldsymbol{x}, \tag{6}$$

where ψ^* is the complex conjugate of the mother wavelet function ψ. To implement equation (6), it is necessary to choose a mother wavelet function ψ first. The Morlet wavelet function, which is a directionally selective and complex-valued wavelet function, is chosen here for detecting the directional wave information from the wave image. The two-dimensional Morlet mother wavelet function, defined in equation (7), and its function in Fourier space, defined in equation (8), was used throughout the implementation procedures in this study:

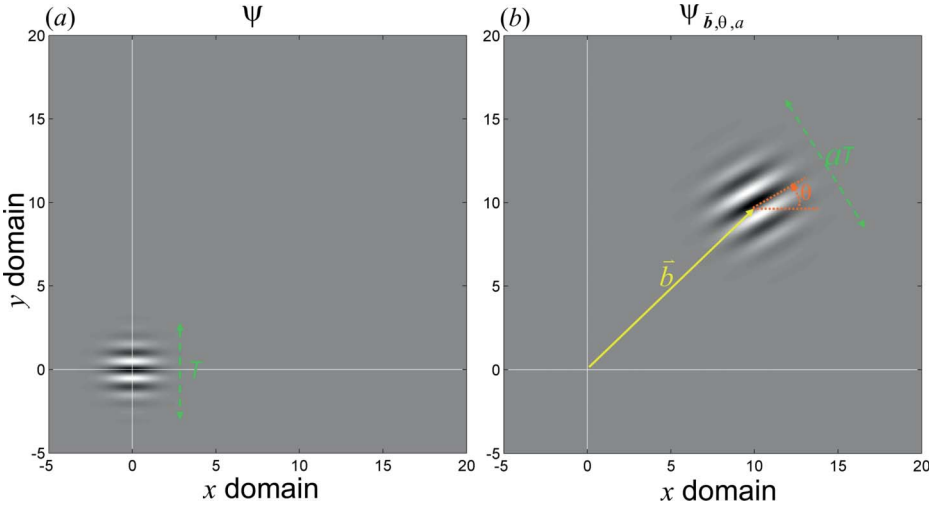

Figure 2. The relationship between mother wavelet function (a) and wavelet function (b).

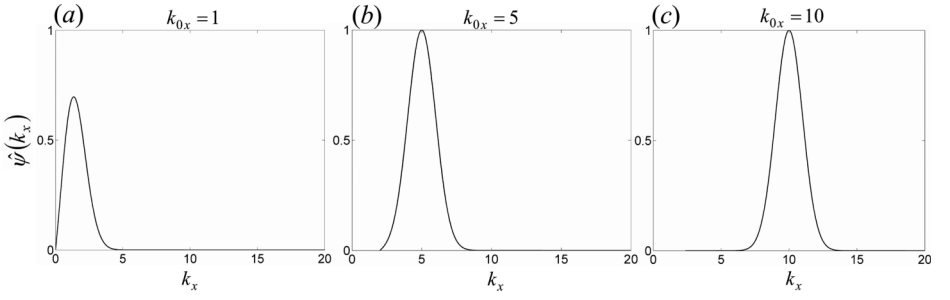

Figure 3. Influence of the parameter k_{0x} upon the wavelet function in the spatial frequency domain.

$$\psi(\boldsymbol{x}) = \mathrm{e}^{-0.5|\mathbf{A}\boldsymbol{x}|^2}\mathrm{e}^{(\mathrm{i}\boldsymbol{k_0}\cdot\boldsymbol{x})} - \mathrm{e}^{-0.5|\mathbf{A}\boldsymbol{x}|^2}\mathrm{e}^{\left(-0.5\left|\mathbf{A}^{-1}\boldsymbol{k_0}\right|^2\right)} \tag{7}$$

and

$$\hat{\psi}(\boldsymbol{k}) = \sqrt{\varepsilon}\left[\mathrm{e}^{-0.5\left|\mathbf{A}^{-1}(\boldsymbol{k}-\boldsymbol{k}_0)\right|^2} - \mathrm{e}^{\left(-0.5\left|\mathbf{A}^{-1}\boldsymbol{k}_0\right|^2\right)}\mathrm{e}^{-0.5\left|\mathbf{A}^{-1}\boldsymbol{k}\right|^2}\right], \tag{8}$$

where $\hat{\psi}$ is the mother wavelet function of ψ in Fourier space, which means that the function is in the frequency (spatial frequency) domain. The spatial frequency, $\boldsymbol{k}$, is the defined wavenumber in the field of oceanography. The parameter $\boldsymbol{k}_0 = (k_{0x}, k_{0y})$ is a vector constant, which is predominant over the oscillations of the wavelet function in the x- and y-directions. Since the oscillations of the wavelet function can be controlled by $\mathbf{r}_{-\theta}$, $k_{0y} = 0$ is used in our study. As shown in figure 3, the peak location of the mother wavelet function in the spatial frequency domain is related to k_{0x}. If the value of k_{0x} is too low, the peak location of the mother wavelet function would be too close to the edge ($k_{0x} = 0$) in the spatial frequency domain. The wavelet function would be incomplete in this case (as shown in figure 3(a)). According to our previous study (Chuang *et al.* 2008), the value of k_{0x} in this study is set up as 6. The matrix $\mathrm{A} = diag[\varepsilon^{-0.5}, 1]$, in which $\varepsilon = 1$ is used here.

2.2 *Basic properties of the 2-D CWT implementation*

A faster algorithm for the 2-D CWT is to calculate in Fourier (spectral) space using the numerical technique of the inverse fast Fourier transform (IFFT), so equation (6) could be calculated using the expression

$$W(\boldsymbol{b}, \theta, a) = C_\psi^{-1/2} a \int_{R^2} \hat{\psi}^*(a\mathbf{r}_{-\theta}(\boldsymbol{k}))\mathrm{e}^{\mathrm{i}\boldsymbol{b}\boldsymbol{k}}\hat{s}(\boldsymbol{k})\mathrm{d}^2\boldsymbol{k}, \tag{9}$$

in which $\hat{s}(\boldsymbol{k})$ is the Fourier transform of $s(\boldsymbol{x})$. $\hat{\psi}_{\boldsymbol{b},\theta,a}(\boldsymbol{k})$ is the function $\psi_{\boldsymbol{b},\theta,a}(\boldsymbol{x})$ in the Fourier space and it is defined as (Antoine *et al.* 1996)

$$\hat{\psi}_{\mathbf{b},\theta,\mathbf{a}}(\boldsymbol{k}) = a\mathrm{e}^{-\mathrm{i}2bk}\hat{\psi}(a\mathbf{r}_{-\theta}(\boldsymbol{k})). \tag{10}$$

Equation (10) shows that the spatial frequency could be transformed from $\boldsymbol{k}$ into $a\mathbf{r}_{-\theta}(\boldsymbol{k})$ after scaling, shifting and rotating a wavelet function. As discussed above, $\boldsymbol{k}_0$ is the peak location of the mother wavelet function in the spatial frequency. After transforming, we assume a new location of the peak energy of the Morlet wavelet function in the Fourier space becomes $\boldsymbol{k}_n$. The relationship between $\boldsymbol{k}_0$ and $\boldsymbol{k}_n$ is given as

$$\boldsymbol{k}_n = \frac{\boldsymbol{k}_0}{a\mathbf{r}_{-\theta}}. \tag{11}$$

As shown in equation (11), the spatial frequency $\boldsymbol{k}_n$ can be obtained by calculating the relationship between $\boldsymbol{k}_0$, a and $\mathbf{r}_{-\theta}$. The spatial frequency $\boldsymbol{k}_n$ stands for the wavenumber, which is an important parameter describing the characteristics of ocean waves. The shifting parameter $\boldsymbol{b}$ of the 2-D CWT stands for the shifting distance of the wavelet function from the original location of the wave-field image. In other words, it presents the analysed location ($\boldsymbol{x}$) of the wavelet function from the image. Hence, the function $W(\boldsymbol{b},\theta,a)$ could be expressed as $W(x,k_n)$ which represents the local image spectrum $W(k_n)$ from different spatial locations $\boldsymbol{x}$.

2.3 *Definition of the non-homogeneity index (I_N)*

The idea of the non-stationarity index from Liu (2000) is applied and modified for calculating the non-homogeneity index from the wave image in our study.

As shown in the previous section, we can obtain the image spectra from different locations of the wave image $W(\boldsymbol{x},\boldsymbol{k}_n)$. For the digital form, $W(\boldsymbol{x},\boldsymbol{k}_n)$ could be presented as

$$W(\boldsymbol{x},\boldsymbol{k}_n) = W(x_j, y_k, k_{xp}, k_{yq}). \tag{12}$$

The averaged image spectrum $\phi(k_{xn},k_{yn})$ from the whole space domain can be obtained from the local spectra from the whole space:

$$\phi(k_{xn},k_{yn}) = \frac{1}{N_x N_y}\sum_{j=1}^{N_x}\sum_{k=1}^{N_y} W(x_j, y_k, k_{xp}, k_{yq}), \tag{13}$$

in which N_x and N_y are the total data samples in the x- and y-directions of the space domain. The idea of the non-homogeneity index (I_N) is similar to the principle of standard deviation in statistics. The deviation between the local image spectrum $W(x_j,y_k,k_{xp},k_{yq})$ and the averaged spectrum $\phi(k_{xn},k_{yn})$ is calculated to obtain the non-homogeneity index, which can be defined as

$$I_N = \sum_{j=1}^{N_x}\sum_{k=1}^{N_y}\sum_{p=1}^{N_{kx}}\sum_{q=1}^{N_{ky}}\left[\frac{W(x_j,y_k,k_{xn},k_{yn}) - \varphi(k_{xp},k_{yq})}{\varphi(k_{xp},k_{yq})}\right]^2, \tag{14}$$

in which N_{kx} and N_{ky} are the total data samples in the spatial frequency domain. For a high non-homogeneous case of a wave image, the local image spectra $W(x_j,y_k,k_{xp},k_{yq})$ should be quite different to different locations (x_j,y_k) of a wave image. Under this situation, the value of the non-homogeneity index should be higher when calculated using equation (14). In other words, the wave image should be more non-homogeneous if the value of the non-homogeneity index is higher.

3. Wave-field image simulation and analysis

To examine the validity of the technique presented above and to test the algorithm, the following numerical simulations of ocean-wave images were performed and discussed.

The numerical simulations were carried out for random waves in which the spectrum of ocean waves was assumed in advance. The irregular wave-field image can be

represented by equation (15). This expression is suitable for a sloped bathymetry (Horikawa 1988):

$$\eta(x,y) = a_{mn} \sum_{m=-M/2}^{M/2} \sum_{n=1}^{N} \sin\left(\int_0^x k_m \cos\theta_n \mathrm{d}x + k_m \sin\theta_n y + \varepsilon_{mn} \right). \tag{15}$$

Here, k_m is the wavenumber of the mth wave component and ε_{mn} is a random phase. The amplitude a_{mn} can be derived from the assumed directional wave spectrum $W(\omega,\theta)$, where ω_m is the wave frequency and θ_n is the wave direction. According to the conservation of energy, the summations of the wave components with different frequencies and directions should be equal to the square of the wave amplitude (equation (16)). The complete algorithm for simulating the ocean-wave spectrum has been proposed by Goda (1999). The input wavenumber is calculated from the dispersion relationship in equation (20), where h is the water depth. The theoretical images spectrum $W(k_x,k_y)$, which will be applied to test the algorithm later, can be transformed from the theoretical wave spectrum $W(\omega,\theta)$ using equation (17) (Tucker and Pitt 2001):

$$a_{mn} = \sum_{m=-M/2}^{M/2} \sum_{n=1}^{N} \sqrt{W(\omega_m,\theta_n)\Delta\omega\Delta\theta} \tag{16}$$

and

$$W(k_x,k_y) = W(\omega,\theta)\frac{1}{k}\frac{\Delta\omega}{\Delta k}. \tag{17}$$

Figure 4 presents an example of a simulated wave image with a significant wave height of 2.5 m, a mean wave period of 8 s and a dominant wave direction of 45 °. The waves move from the northwest. Due to the influence of the variable bathymetry upon the wave propagation, wave direction and wavenumber change with space (Chuang *et al.* 2008).

As discussed above, the wave image should be more non-homogeneous if the value of the non-homogeneity index is higher. As shown in equations (13) and (14), the local image spectrum $W(\boldsymbol{x},\boldsymbol{k}_n)$ is the key to calculating the non-homogeneity index. The local image spectrum was calculated using the 2-D CWT. It is necessary to check the accuracy of the image spectrum so as to ensure the correctness of the non-homogeneity index. By applying the 2-D CWT on the simulated wave image, the image spectra at six locations, marked in figure 4, were derived and projected onto the spatial frequency domain (wavenumber plane) to present energy contours, as shown in figure 5.

Figure 5 shows the wavenumber corresponding to energy contour at location 1 (deeper water) and gradually moves from a lower value to a higher one at location 6 (shallow water). The dominant wave directions also change with water depth. Each contour corresponds to one wave component and its mirror image in the opposite direction. It means that the wave directions are ambiguous in judging the 180° difference when a single wave image is transformed for the image spectrum. The ambiguity could be eliminated by adopting a series of wave images (Young *et al.* 1985). The theoretical wavenumber and wave direction conditions, which are input into the algorithm of the wave-field simulation, are also marked by the plus signs on the image spectra of figure 5. The location of the contour peak should be close to the plus sign if the local image spectrum by the 2-D CWT is accurate enough. As shown in

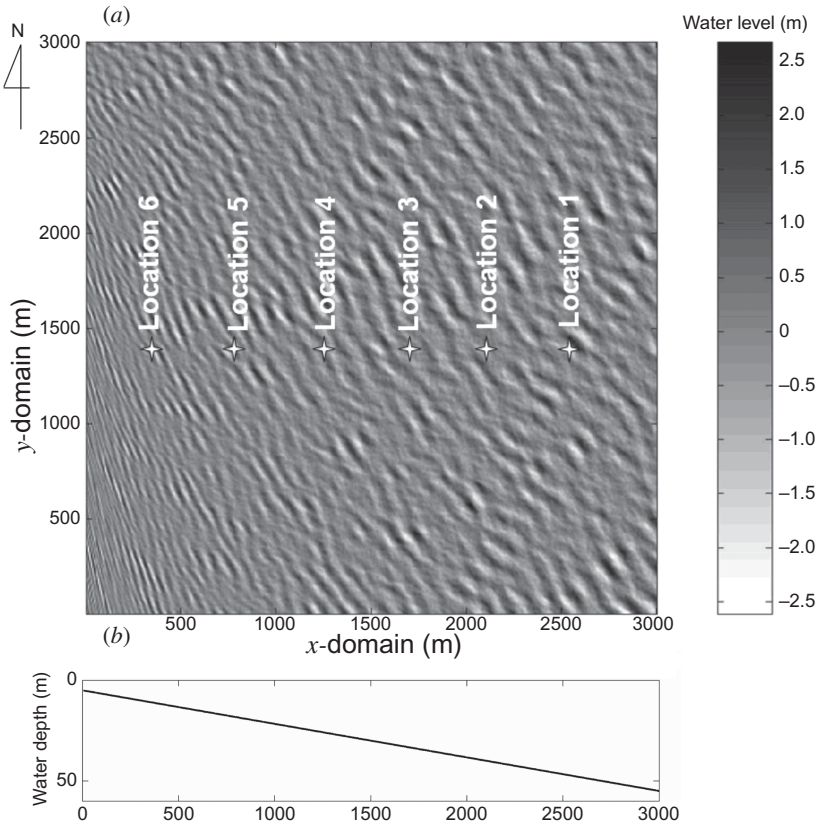

Figure 4. Simulated random wave-field image on a slowing varying topography.

figure 5, the plus sign almost overlaps the contour peak on the local wave image spectrum from location 2 to location 5. The calculated results of the wave parameters (figure 6) from different locations by the 2-D CWT also show that the accuracies were poor at location 1 and location 6. It could be due to the influence of the edges of the wave-field image upon wave analysis, which can be explained using figure 7. As shown in equation (2), the 2-D CWT is the inner product of the wavelet function and the image function. However, the wavelet function is not complete at the locations of interest near the edges of the image because its energy distribution is cut off there. After applying this incomplete wavelet function to the wave image analysis, the spectral energy is biased. The errors were more conspicuous at location 1 and location 6 of the wave image than in other locations.

Different kinds of wave images were simulated and analysed for understanding the influence of the image edges upon calculating the wave. Figure 8 shows that the calculated errors would decrease if the analysed locations were distant from the image edges. The distance between the image edge and analysed location is related to the dominant wavelength of the wave field. The normalized root mean square error of the wave calculations would be lower than 5% if the distance between the image edges and calculated locations were larger than half the wavelength of the wave field.

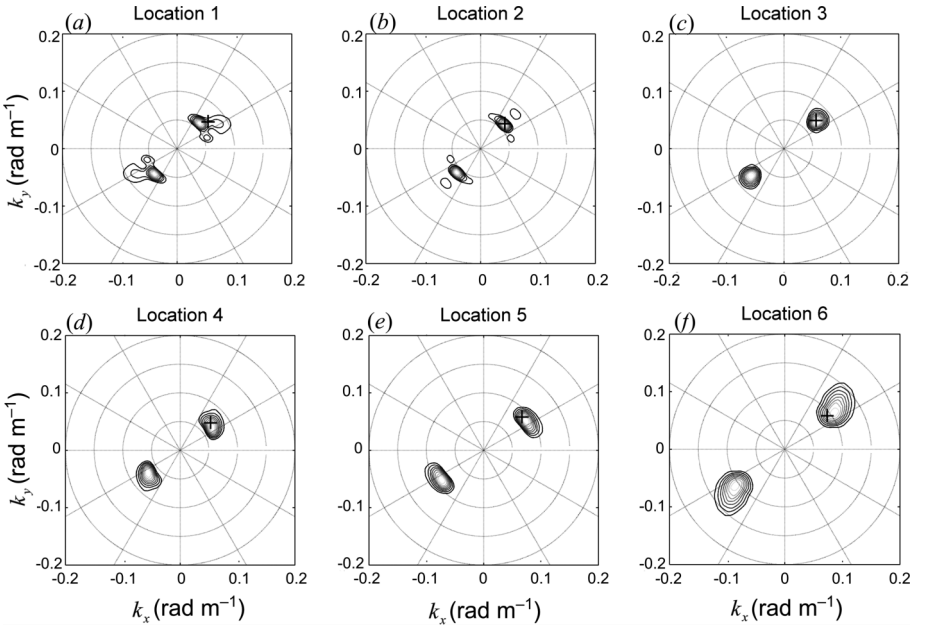

Figure 5. Wavenumber contours estimated by the wavelet transform at six locations of the wave-field image (figure 4).

4. Discussion

We have shown the accuracy of the local image spectra from a non-homogeneous wave-field image using the 2-D CWT above. In this section, we discuss the non-homogeneity indexes under different conditions. Figure 9 shows the non-homogeneity indexes of the wave cases with different gradients (sea bed slopes = 0–0.015) in the bathymetry. The value of the non-homogeneity index increases with space except for the case of a horizontal sea bed ($S = 0$). It is revealed that the non-homogeneity index is related to the gradient in the bathymetry. For the wave-field case on a steeper seabed, waves transform their characters rapidly (Dean and Dalrymple 1991). Wave field would be more inhomogeneous in this case. It is the reason that the value of the non-homogeneity index is higher under the situation of steeper sea bed.

Different non-homogeneity indexes are calculated from these simulated image cases using the 2-D CWT algorithm. For the traditional image-analysing methods, e.g. the Fourier transform, the averaged spectrum $S(k_x, k_y)$ is obtained from the whole wave-field image. Wave parameters, such as wavenumber k and wave direction θ can be calculated from the wave image spectrum:

$$k = \sqrt{k_x^2 + k_y^2} \tag{18}$$

and

$$\theta = \tan^{-1}(k_x/-k_y). \tag{19}$$

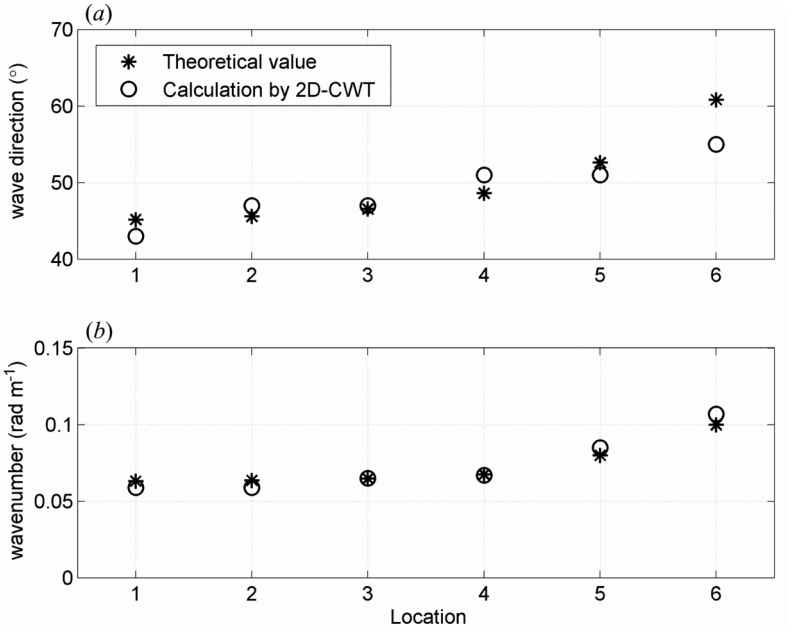

Figure 6. Wave parameters for analysing the results obtained from different locations (figure 4).

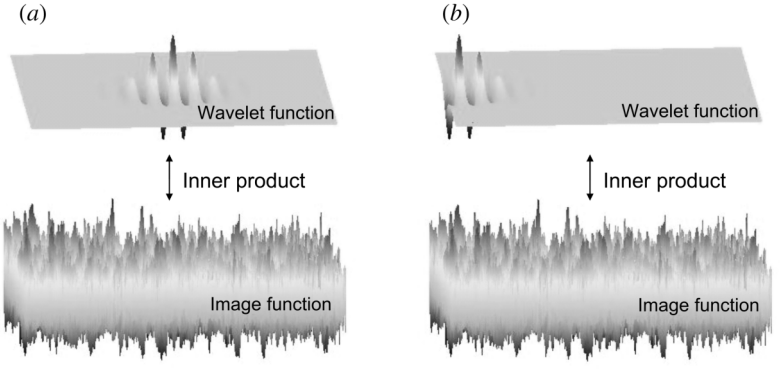

Figure 7. A schematic illustration of a wavelet function performed on the marginal area of an image function.

The wave features in the spatial frequency domain can be described by one averaged spectrum from the whole wave-field image. However, the wave features are variant with space for the cases of inhomogeneous wave-field images. The deviations between the averaged results from the Fourier transform and the theoretical wave values from different locations of the entire non-homogeneous wave-field image were calculated. These show that the higher the non-homogeneity index, the higher the deviations between the averaged results using the Fourier transform and the theoretical wave parameters from the entire non-homogeneous wave-field image (figures 10 and 11). According to the Heisenberg Uncertainty Principle (Van Name

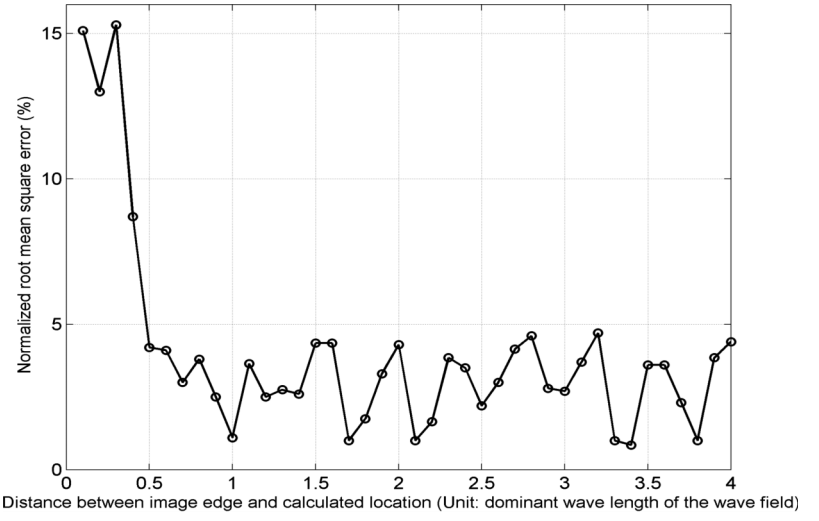

Figure 8. The normalized root mean square error of the wave calculations from different distances between the image edge and the calculated locations.

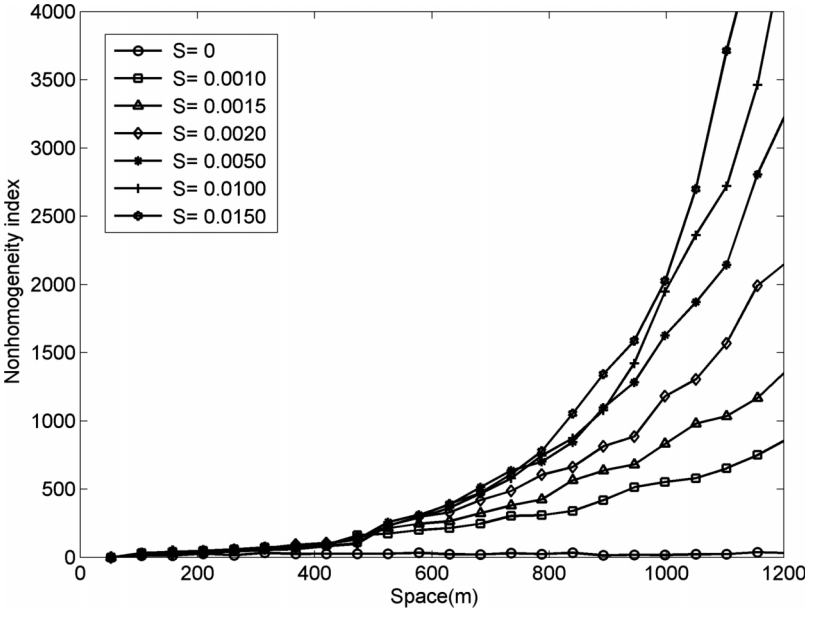

Figure 9. Non-homogeneity indexes with different gradients in the bathymetry.

1960), the resolution of the image spectrum should be high enough using the Fourier algorithm. For the cases of low non-homogeneity index from the wave images, the wave characteristics would not change obviously with space. The Fourier transform would be suitable for analysing the wave images, in order to obtain better resolutions

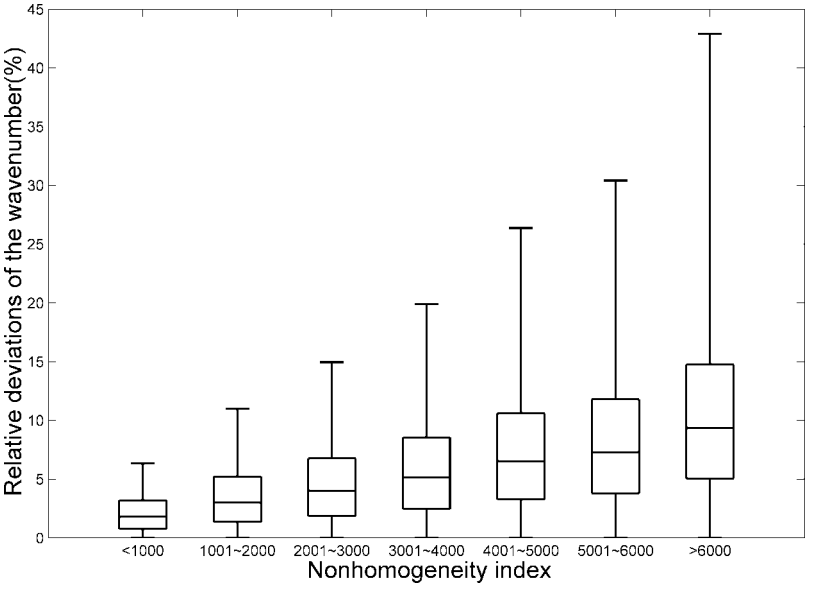

Figure 10. Relative deviations of the wavenumber between the results from the Fourier transform and from the theoretical values.

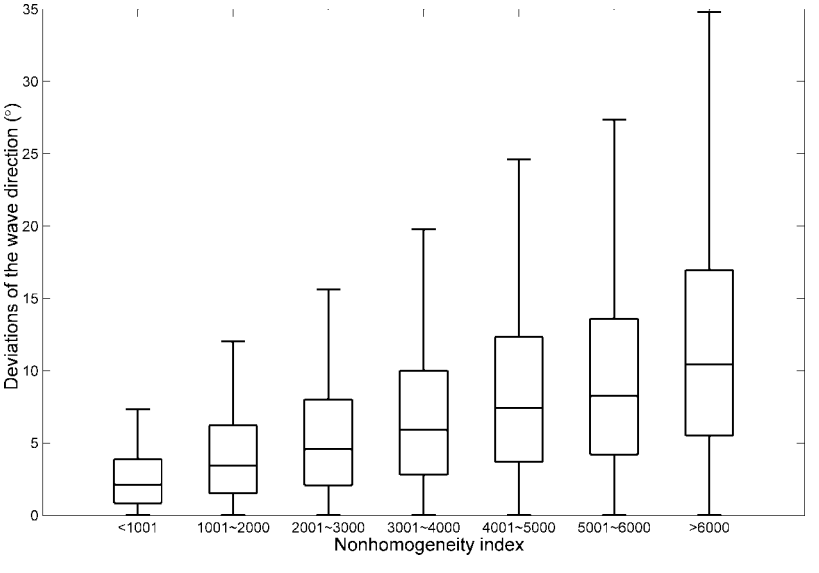

Figure 11. Deviations of the wave direction between the results from the Fourier transform and between the theoretical values from the wave image.

in the spatial frequency domain. However, the inhomogeneous algorithm, i.e. the CWT, should be more appropriate for cases of high non-homogeneity indexes.

5. Natural wave-field images analysis

As discussed above, the non-homogeneity was tested using the simulated wave image. In order to verify the practicality of the algorithm on natural signals, X-band radar images observed from the sea surface were applied here. The X-band radar is one of the prevalent systems for observing ocean waves, and it has been shown that it is possible to obtain reliable data of wave characteristics after comparing with corresponding buoy data (Nieto Borge and Soares 2000). The X-band radar is suitable for monitoring the waves in near-offshore or shallow zones. For applications of coastal engineering, coastal-area protection and management and oceanic recreation, the interesting area is always within several kilometres of the land and has a high measurement resolution requirement. The X-band radar should be an ideal tool to cope with this situation. Radar images are generated by the interaction of electromagnetic waves with sea-surface ripples at grazing incidence. Radar backscatter is presented as a grey value. Although the backscatter energy from radar images is not indicative of the elevation of sea-surface level, it has been, until now, the popular way to obtain near-wave information in space domains from field measurement (Nieto Borge *et al.* 1999, Barale and Gade 2008).

In this study, the radar images were observed in the southern Taiwan Kenting Sea area (figure 12). The water depth in the analysed area ranges from 10 to 100 m. About 200 radar image cases are applied here. Three different areas, as shown in figure 12, are selected for analysing the non-homogeneity indexes. Figure 13 shows that the calculated results of the non-homogeneity indexes from deep-water areas are smaller than those from the shallower water areas. According to linear ocean-wave theories, wavenumber and wave direction are influenced by the water depth (h):

$$\omega^2 = gk \tanh(kh) \tag{20}$$

and

$$k \sin\theta = \text{const.}, \tag{21}$$

in which ω is the wave frequency, which is constant during the wave propagation based on known linear wave theories. k and θ are described above and g is the acceleration due to gravity. For the deep-water area, the term $\tanh(kh)$ in equation (20) approximates to 1. In other words, wavenumber and wave direction would be nearly constant during wave propagation in deep-water situations. This is the reason why the non-homogeneity indexes in area A of the radar wave field are smaller than that in other areas. It does conform to the ocean-wave theories.

6. Conclusions

Ocean-wave observation plays an important role in the fields of ocean engineering and marine science. Remote sensing is a useful way to present ocean-wave features in the space domain. Fourier transforms were applied frequently to calculate the wave image spectra from ocean remote-sensing images under the assumption that wave features within the image are homogenous. However, ocean-wave information from remote-sensing images is always inhomogeneous. In order to obtain complete and

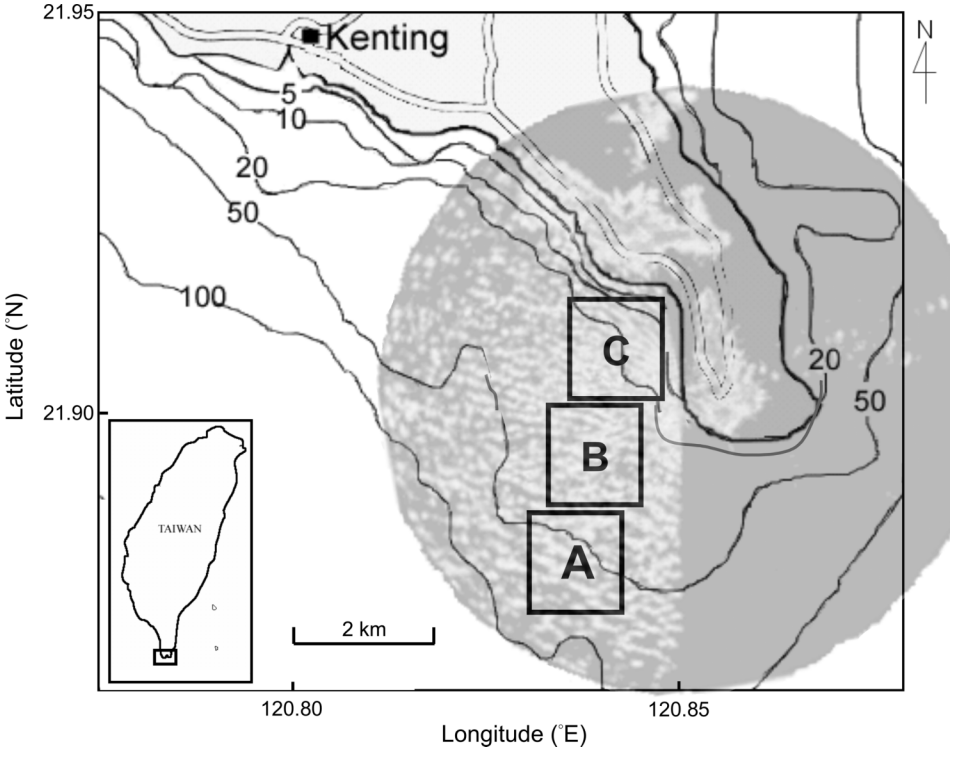

Figure 12. The natural wave-field image and its corresponding bathymetry.

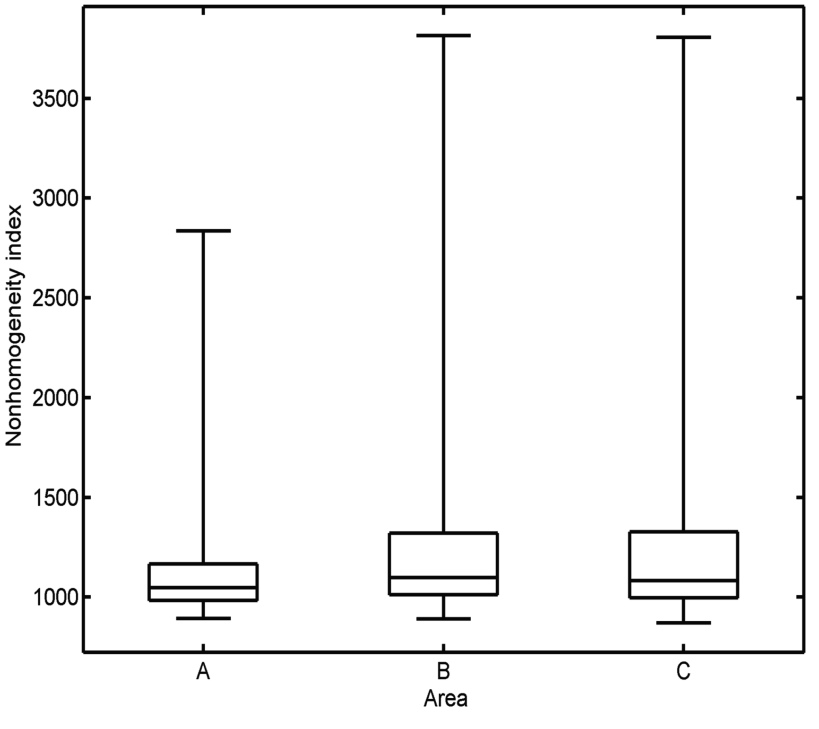

Figure 13. The non-homogeneity indexes from the different areas in figure 12.

reliable wave information, it is necessary to determine the degree of non-homogeneity degree of the analysed image. This study was aimed at developing an algorithm for quantifying the non-homogeneity from the ocean-wave remote-sensing images, so as to determine the homogeneous areas from the wave image.

The algorithm for quantifying the non-homogeneity from the image was based on the 2-D CWT. To examine the validity of the algorithm, the numerical simulated wave images were performed and discussed. The 2-D CWT is capable of extracting the local image spectrum, which is the key to quantifying non-homogeneity, at any chosen location from the wave-field image. However, the accuracy of the local image spectrum is influenced by the edges of the image. The distance between the image edges and the chosen locations should be larger than half the wavelength of the waves in calculating the highly accurate image spectrum.

According to the calculated results of the non-homogeneity indexes from different kinds of simulated images, it was revealed that the gradient in the bathymetry is the key that influences the values of non-homogeneity index from the wave images. In addition to the simulated wave-field images, X-band radar images observed from the ocean surface were also applied for exploring non-homogeneity wave fields in nature. The observed wave fields from different cases of the bathymetry were discussed. The results reveal that the non-homogeneity indexes are higher in the cases of shallow water areas; this conforms to ocean-wave theories.

In this study, we have proved that the non-homogeneity index is capable of presenting the degree of wave non-homogeneity. Based on our results, it is suggested that the inhomogeneous algorithm would be more appropriate for the case of high non-homogeneity indexes.

Acknowledgements

This work was supported by the Ministry of Education, Taiwan, ROC under the NCKU Project of Promoting Academic Excellence & Developing World Class Research Centers. The radar images are provided by the Water Resources Agency in Taiwan, ROC. The authors would like to offer the great thanks to the agencies. In addition, the authors are grateful to the referees for helpful comments and suggestions.

References

Alpers, W. and Hasselmann, K., 1978, The two-frequency microwave technique for measuring ocean-wave spectra from an airplane or satellite. *Boundary-Layer Meteorology*, **13**, pp. 215–230.

Antoine, J.-P., Vandergheynst, P., and Murenzi, R., 1996, Two-dimensional directional wavelets in image processing. *International Journal of Imaging Systems and Technology*, **7**, pp. 152–165.

Antoine, J.-P., Murenzi, R., Vandergheynst, P. and Twareque Ali, S., 2004, *Two-dimensional Wavelets and their Relatives* (Cambridge, UK: Cambridge University Press).

Barale, V. and Gade, M., 2008, *Remote Sensing of the European Seas* (The Netherlands: Springer).

Chuang, L.Z.H., Wu, L.C., Doong, D.J. and Kao, C.C., 2008, Two-dimensional continuous wavelet transform of simulated spatial images of waves on a slowly varying topography. *Ocean Engineering*, **35**, pp. 1039–1051.

Dean, R.G. and Dalrymple, R.A., 1991, *Water Wave Mechanics for Engineers and Scientists* (Singapore: World Scientific Publishing Co.).

Goda, Y., 1999, A comparative review on the functional forms of directional wave spectrum. *Coastal Engineering Journal*, **41**, pp. 1–20.

Horikawa, K., 1988, *Nearshore Dynamics and Coastal Processes – Theory, Measurement, and Predictive Models* (Tokyo, Japan: University of Tokyo Press).

Kanevsky, M.B., 2005, New spectral estimate for SAR imaging of the ocean. *International Journal of Remote Sensing*, **26**, pp. 3707–3715.

Kuo, Y.Y., Leu, L.G. and Kao, Y.L., 1999, Directional spectrum analysis and statistics obtained from ERS-1 SAR wave images. *Ocean Engineering*, **26**, pp. 1125–1144.

Liu, P.C., 2000, Is the wind wave frequency spectrum outdated. *Ocean Engineering*, **27**, pp. 577–588.

Mountain, R.D. and Birnbaum, G., 1982, Inhomogeneity size and shape determination from scattering of low frequency sound waves. *Journal of Applied Physics*, **53**, pp. 3581–3584.

Nieto Borge, J.C. and Soares, C.G., 2000, Analysis of directional wave fields using X-band navigation radar. *Coastal Engineering*, **40**, pp. 375–391.

Nieto Borge, J.C., Reichert, K. and Dittmer, J., 1999, Use of nautical radar as a wave monitoring instrument. *Coastal Engineering*, **37**, pp. 331–342.

Priestley, M.B., 1991, *Non-Linear and Non-Stationary Time Series Analysis* (London, UK: Academic Press Limited).

Reeve, D., Chadwick, A. and Fleming, C., 2004, *Coastal Engineering: Processes, Theory, and Design Practice* (New York, NY: Spon Press).

Tucker, M.J. and Pitt, E.G., 2001, *Waves in Ocean Engineering* (Oxford, UK: Elsevier Science Ltd).

Turiel, A., Isern-Fontanet, J.,Garcia-Ladona, E. and Young, J.A., 2007, Detection of wave fronts in the Indian Ocean from geostationary sunglint satellite imagery. *International Journal of Remote Sensing*, **28**, pp. 3953–3962.

Vachon, P.W. and West, J.C., 1992, Spectral estimation techniques for multilook SAR images of ocean waves. *IEEE Transactions on Geoscience and Remote Sensing*, **30**, pp. 568–577.

Van Name, F.W., 1960, *Modern Physics* (New Jersey, NJ: Englewood Cliffs).

Young, I.R., Rosenthal, W. and Ziemer, F., 1985, A three-dimensional analysis of marine radar images for the determination of ocean wave directionality and surface currents. *Journal of Geophysical Research*, **90**, pp. 1049–1059.